

# Wireless Stimulation of Motor Cortex Through a Collagen Dura Substitute Using an Ultra-Thin Implant Fabricated on Parylene/PDMS

Abed Benbuk<sup>1</sup>, Graduate Student Member, IEEE, Daniel Gulick<sup>1</sup>, Member, IEEE, Diogo Moniz-Garcia<sup>2</sup>, Shiyi Liu<sup>1</sup>, Member, IEEE, Alfredo Quinones-Hinojosa<sup>2</sup>, and Jennifer Blain Christen<sup>1</sup>†, Senior Member, IEEE

**Abstract**—We present the design, fabrication, and *in vivo* testing of an ultra-thin (100 μm) wireless and battery-free implant for stimulation of the brain's cortex. The implant is fabricated on a flexible and transparent parylene/PDMS substrate, and it is miniaturized to dimensions of 15.6×6.6 mm<sup>2</sup>. The frequency and pulse width of the monophasic voltage pulses are determined through On-Off keying (OOK) modulation of a wireless transmission at 2.45 GHz. Furthermore, the implant triggered a motor response *in vivo* when tested in 6 rodents. Limb response was observed by wireless stimulation of the brain's motor cortex through an FDA-approved collagen dura substitute that was placed on the dura in the craniotomy site, with no direct contact between the implant's electrodes and the brain's cortical surface. Therefore, the wireless stimulation method reported herein enables the concept of an e-dura substitute, where wireless electronics can be integrated onto a conventional dura substitute to augment its therapeutic function and administer any desired stimulation protocol without the need for post-surgical intervention for battery replacement or reprogramming stimulation parameters.

**Index Terms**—Wireless, Battery-free, Implant, Brain, Cortical Stimulation, Dura Substitute, e-dura, Wireless Power Transfer (WPT).

## I. INTRODUCTION AND BACKGROUND

**F**LEXIBLE neural implants with neuromodulation capability hold great promise and could potentially transform the diagnosis and treatment of multiple neurological disorders, such as epilepsy, tumor, and movement disorders, and assist with recovery of function. [1]–[3]. Stimulation-capable implants have been used with considerable success in epilepsy, and movement disorders, including essential tremor and Parkinson's disease. Moreover, they have been proposed and tested for treating mood disorders, such as depression. More recently, stimulation has been shown to induce neural plasticity in glioma patients, suggesting potential future applications for patients with tumors infiltrating eloquent brain regions [4]. Nevertheless, significant challenges and known complications with the current generation of devices have hindered their wider adoption. These include wire failure

<sup>1</sup>Abed Benbuk, Daniel Gulick, Shiyi Liu, and Jennifer Blain Christen are with the Department of Electrical, Computer, and Energy Engineering, Arizona State University, Tempe, Arizona, USA. (email: {abenbuk, dgulick, sliu148, Jennifer.Blainchristen}@asu.edu).

<sup>2</sup>Diogo Moniz-Garcia and Alfredo Quinones-Hinojosa are with the Department of Neurologic Surgery, Mayo Clinic, Jacksonville, Florida, USA. (email: {Garcia.Diogo, Quinones-Hinojosa.Alfredo}@mayo.edu).

†Corresponding author.

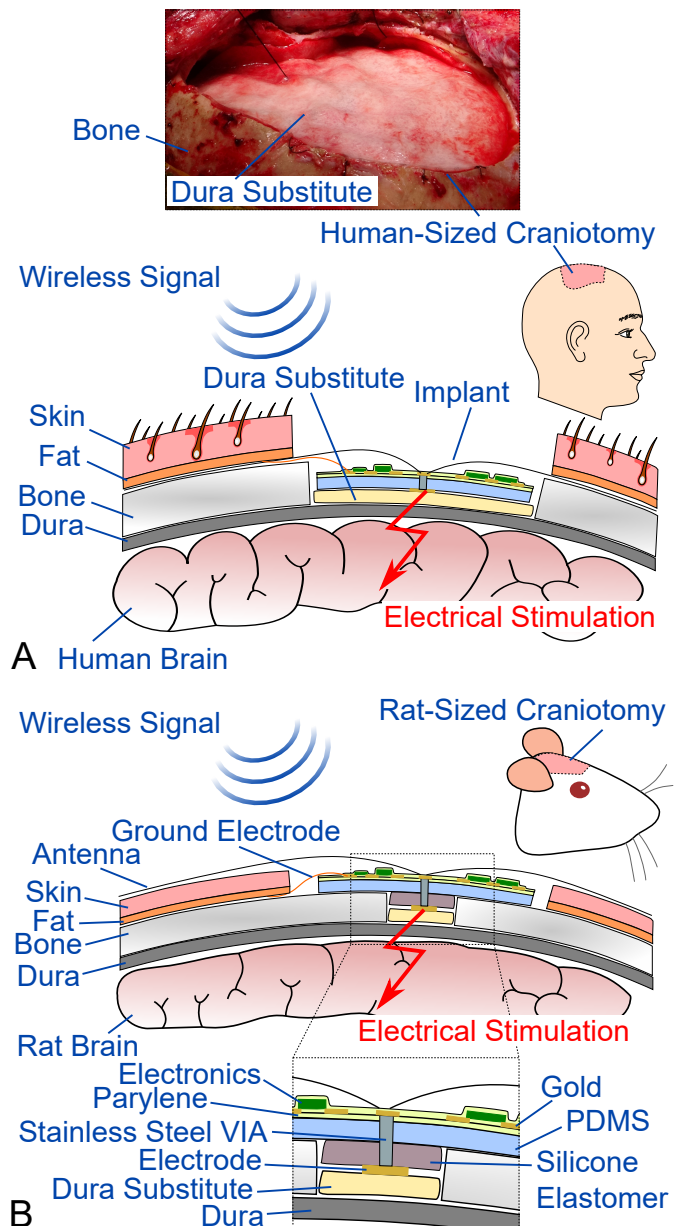


Fig. 1. A graphical rendering of the e-dura substitute concept. A) The envisioned human implementation with the implant entirely positioned on the dura substitute. B) The *in vivo* test setup used in this study utilizes a rat-sized craniotomy with the implant positioned on the bone. The dimensions shown are not to scale.

and migration, hardware infection that necessitates revision surgery, and battery replacement surgeries [5], [6]. Several studies have been conducted on the prevalence of complications that impact patients with biomedical implants. A recent study [7] has revealed that infections, wire movement, and wire failure are the top three reasons for surgical re-interventions in patients with brain implants. Similar conclusions were reached in a study on complications in patients with cardiac pacemakers [8]. These findings have motivated efforts to develop wireless implants, given their potential to reduce complications and prevent battery replacement surgeries [9]–[12]. Novel embodiments or placement techniques are also needed to reduce the risk of hardware migration and the morbidity of current placement strategies. Wireless implants rely on wireless power transfer (WPT) to deliver power from an external transmitter to an implant that is equipped with the necessary electronics to harvest, store, and deliver monophasic or biphasic voltage pulses [13]–[16]. The wireless signal can vary in frequency between several megahertz to several gigahertz [17]–[20]. Delivering power at a higher frequency allows reduced size of the transmit and receive antennas, at the expense of increased signal attenuation in lossy tissue media [21]. Voltage pulses with at least a few volts are required for most stimulation protocols. To meet these requirements, the implant may contain a passive rectifier [22], a microcontroller [17], or CMOS integrated circuitry [23], [24]. Within the past few decades, current-controlled neurostimulator designs have become favored over constant-voltage designs, in order to reduce stimulation variance caused by electrode impedance changes.

Ensuring implant biocompatibility is a major consideration, typically achieved by a biocompatible coating [22] or enclosure [25] that acts as a barrier between non-biocompatible and stiff substrates (such as FR4) and conductive materials (such as copper or silver epoxy) that constitute the implant and the surrounding tissue. The use of coatings and enclosures usually results in an undesirable increase in thickness. Moreover, the use of large electronics, such as microcontrollers, results in varied topography and increases the peak thickness of the implant even when the substrate is extremely thin [26]. Therefore, it is still challenging to develop adequately thin implants to enable their placement in real clinical scenarios. Flexible and conformal substrates and malleable conductive materials have attracted notable interest as they reduce bending stiffness and consequent stress between the device and tissues, [1], [27] enabling safer placement and long-term use. Examples of soft substrate materials include polyimide [18], [26] and soft elastomers [15]. Polydimethylsiloxane (PDMS) is a biocompatible, soft, and transparent material which makes it a popular solution as a coating. It is typically used to shield implants through dip-coating [28] but its use as the main implant substrate remains insufficiently investigated due to its incompatibility with high-temperature fabrication processes and weak attachment to metals. Additionally, PDMS is not a popular high-frequency substrate material due to its low relative permittivity ( $\epsilon_r = 3$ ) and high loss tangent (0.019 @ 2.4 GHz) [29]–[31]. Therefore, additional studies are needed to explore the potential of PDMS as a substrate.

The dura mater is an essential component of the meninges that isolate the central nervous tissue. The dura can often be invaded or damaged within the context of infiltrative diseases, trauma, and others. Collagen dura substitute is a commonly used material that is employed to repair or replace damaged or removed dura [32]. Non-degradable dura substitute material is used as an artificial barrier between the brain and the surrounding tissue [32]. The dura substitute offers desirable mechanical properties such as resistance to tear and leakage of cerebrospinal fluid [33]. These properties make the collagen dura substitute an attractive platform for wireless electronics that can be integrated and made available in personalized designs to fit surgical planning. The electrical properties of collagen, including impedance magnitude and phase, conductivity, and relative dielectric permittivity were studied in [34]. The results show that collagen solutions are characterized by an impedance magnitude in the range of 1 to 3 k $\Omega$  depending on the concentration of collagen in the solution.

In this study, we present the design, fabrication, and *in vivo* testing ( $n = 6$  rodents) of a wireless, battery-free brain stimulator implant. The implant is realized on a parylene/PDMS substrate with a thickness of 100  $\mu\text{m}$  and a peak thickness of 0.61 mm. Stimulation is externally controlled to determine the frequency and pulse width of the monophasic pulses without the need for intervention to reprogram these parameters. Furthermore, we propose the e-dura substitute as a novel stimulation method that eliminates contact between the implant and the cortical surface by delivering adequate current through an FDA-approved surgical dura substitute. The e-dura substitute concept is shown in Fig 1A. In our envisioned human implementation, a dura substitute is inserted to seal the craniotomy site and facilitate recovery after surgery, and the implant is placed on top of the dura substitute before the overlying bone flap is replaced. The implant integration on top of the dura substitute allows electrical brain stimulation without direct contact with the brain's cortical surface. The *in vivo* testing setup (Fig. 1B) contains a piece of dura substitute that is inserted into a rat-sized craniotomy and part of the implant is positioned on top of the bone. The implant makes contact with the dura substitute through a soft silicone pedestal to deliver cortical electrical stimulation. The e-dura substitute proposed herein enables surgeons to administer a multi-functional solution that combines the role of a mechanical barrier and the well-known therapeutic effects of a dura substitute with electrical stimulation for improved recovery.

## II. MATERIALS AND METHODS

### A. External Transmitter

The external transmitter contains the necessary components to deliver power to the wireless implant and control the parameters of the monophasic voltage stimulation pulses. These parameters include amplitude, frequency, and pulse width. As shown in Fig. 2, the external transmitter comprises an RF signal source (5009, Valon) that generates a continuous wave radio frequency (RF) signal at 2.45 GHz. A power amplifier (MPA-24-20, RF Bay, Inc) boosts the RF power level that

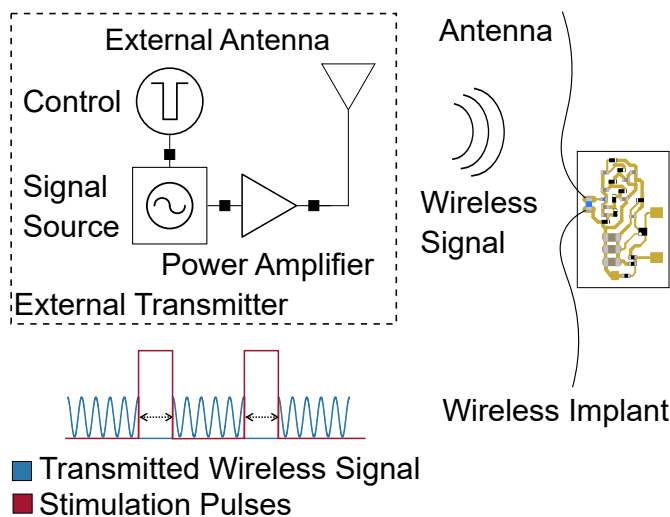


Fig. 2. A block diagram showing the operating principle of the wireless implant. The external transmitter determines the stimulation protocol by OOK-modulation of the wireless signal.

is radiated by an external antenna (A10194, Antenova). The maximum transmitted power level is always kept well below 30 dBm in the benchtop and *in vivo* experiments to comply with FCC regulations [35] which require that the maximum Effective Isotropic Radiated Power (EIRP) not exceed 30 dBm for a variety of applications. An On-Off-Keying (OOK) signal controls the wireless transmission. During the ON periods, the external transmitter delivers wireless power to the implant to replenish its energy storage. The implant generates monophasic stimulation pulses during the OOK OFF period, delivering the stored energy through the electrodes. The stimulation pulse width is approximately equal to the OOK OFF period. The implant remains idle if the OOK transmission ceases. This approach enables on-demand operation and the ability to change stimulation parameters anytime after the implant is placed on the dura substitute.

### B. Wireless Implant Circuit

The implant receives wireless power through a dipole antenna, and it contains a rectifier, energy storage capacitors, and a P-MOSFET to generate stimulation pulses. The implant circuit diagram is shown in Fig. 3. A Dickson voltage multiplier rectifies and boosts the received wireless signal. It comprises several Schottky diodes (D1-D8, JDH2S02SL, Toshiba) and smoothing capacitors (C1-6, 10 pF, Murata). The number of stages was selected to achieve a balance between high output voltage and a small footprint. An impedance-matching inductor (L1, 2.2 nH) cancels the negative imaginary impedance at the input of the Dickson multiplier to minimize the input reflection coefficient seen by the antenna looking into the rectifier. Large Signal S-parameters (LSSP) and Harmonic Balance (HB) simulations were used to find the input impedance of the rectifier circuit and determine an initial value for the optimal matching inductor at 3 nH (Advanced Design System 2021, Keysight). A detailed description of the simulation testbench is provided in Supplementary Material

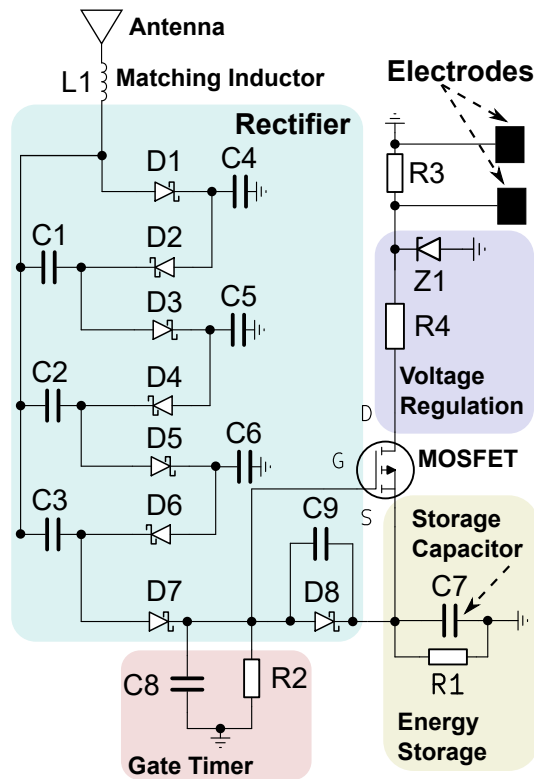


Fig. 3. A detailed circuit diagram of the wireless implant. It contains a Dickson voltage multiplier that converts the wireless signal into DC voltage that is delivered to the load through a P-MOSFET switch. An optional voltage regulation stage can be added to limit the output voltage.

Fig. S1. The optimal matching inductor value was optimized experimentally as shown in Supplementary Material Fig. S2 by comparing the output voltage of several identical implants equipped with different values of matching inductors. A timer circuit (C8 R2) is applied to the gate of the P-MOSFET (PMZ320UPEYL, Nexperia). It charges during the OOK ON intervals and to a voltage that matches the voltage formed across the energy storage capacitor (C7, 30  $\mu$ F, Murata). Therefore,  $V_{GS} \approx 0$  and no current is delivered to the load resistor (R3, 10 k $\Omega$ ). At the onset of the OOK OFF intervals, the timer circuit discharges, and current is delivered through the drain-source channel to the load. A 2.45 GHz signal can be coupled directly to the traces from the external antenna. This signal is rectified if it appears in parallel with diode D8 which leads to an unwanted DC offset at the MOSFET gate. Therefore, an RF short capacitor (C9, 20 pF) is connected in parallel across diode D8 to short the coupled 2.45 GHz signal and ensure that the gate is only biased using the gate timer circuit. In addition, this capacitor is a DC block that keeps the DC voltage at C7 from appearing at the MOSFET gate.

An optional voltage regulation circuit can be implemented at the output to limit the amplitude of the stimulation pulses and ensure safety. It is composed of a Zener diode (Z1) with a specific voltage ( $V_Z$ ) that is determined by the medical application, and a tuning resistor (R4) to determine the regulated input voltage range. An example implementation of the voltage regulation circuit is discussed in Supplementary Material Fig. S3. Recent neurostimulator designs have favored current-

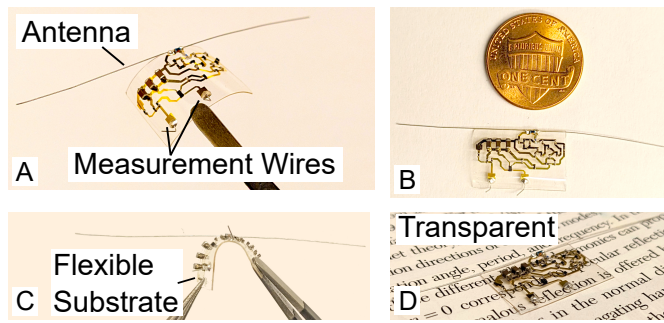


Fig. 4. Photographs of the fabricated wireless implant, highlighting its various mechanical properties. A) The implant is fabricated on a 100  $\mu\text{m}$ -thick Parylene/PDMS substrate. B) The implant is miniaturized to dimensions suitable for testing in rat models. C) The flexible substrate shows good tolerance to bending. D) The combination of Parylene/PDMS maintains transparency, allowing clear observation of text.

controlled stimulation, rather than voltage-controlled, in order to deliver more consistent treatment over time by reducing the variations due to electrode impedance changes [36]. For this work, the more conventional voltage-controlled design was chosen in order to minimize the number and complexity of components needed. Regardless of whether current- or voltage-controlled, neurostimulation intensity must be adjusted in order to achieve the desired effect given the exact location of the electrode relative to the targeted neural structures. The Zener diode regulation scheme proposed in this work is also different from conventional constant-voltage stimulation because the voltage is fixed. To adjust the stimulation for each animal's specific motor threshold, the pulse duration can be changed. This interaction between stimulation intensity and pulse length is well-described by the strength-duration curve [37].

### C. Wireless Implant Fabrication

The implant is fabricated on a silicon wafer in a low-temperature process that is described in detail in Supplementary Material Fig. S4. Various properties of the implant are highlighted in the pictures shown in Fig. 4. The pictures are taken before step (I) in the fabrication process shown in Supplementary Material Fig. S4. Polydimethylsiloxane (PDMS) ( $\epsilon_r = 3$ ) forms the main substrate (100  $\mu\text{m}$ ) on top of which gold traces interconnect the implant circuit. A parylene interface layer (8  $\mu\text{m}$ ) is added between the PDMS and the gold layer to enhance the adhesion of gold to the PDMS substrate while maintaining flexibility and transparency. This combination of two dielectric materials was chosen because parylene alone is not transparent at a thickness that provides strong structural support. On the other hand, PDMS cannot be solely used as a main substrate because it does not exhibit good attachment to gold. While other methods exist for enhancing the adhesion of gold to PDMS, we rely on parylene because it offers other desirable properties, such as low permeability to moisture (Dimer C). In our previous work [38], we found that the combination of parylene/PDMS maintains excellent transparency with a parylene layer thickness of up to 20  $\mu\text{m}$ . Clear observation of cultured human-derived cardiomyocytes

was possible using an inverted fluorescence microscope (Axio Observer Z1, Zeiss). A parylene passivation layer (2  $\mu\text{m}$ ) is added to protect and electrically isolate the electronics. A soft silicone elastomer pedestal is then attached to the bottom of the implant, underneath the positive electrode to fill the gap between the skull and the dura substitute for testing in a rat model. The pedestal has a thickness that is similar to the rat's skull (1 mm) and it allows the implant to be positioned on the bone during *in vivo* testing. Electrical stimulation is delivered from the top layer through a stainless steel VIA to a gold-plated disk electrode with a diameter of 1.2 mm that is attached using silver epoxy to the silicone elastomer pedestal. Detailed steps describing the electrode fabrication, and photographs of the implant with the integrated electrode are shown in Supplementary Material Fig. S5. The assembly process for the human implementation may not require the silicone elastomer (see Fig. 1) if the implant can entirely fit on the dura substitute. Instead, only a VIA and a similar electrode with possibly a larger diameter can be used.

The antenna is formed of two coated and flexible stainless wires each with a length of 25 mm and diameter of 127  $\mu\text{m}$ , as seen in Fig. 4A. Measurement wires are connected to the implant for data acquisition. The implant's circuit is miniaturized as shown in Fig. 4B, and it occupies an area of  $15.6 \times 6.6 \text{ mm}^2$  which allows *in vivo* testing in a rat model. Combining soft dielectric materials with gold, a malleable metal, results in good tolerance to bending as shown in Fig. 4C. The implant maintains transparency, allowing clear observation of the text underneath, as shown in Fig. 4D. These mechanical properties make the implant a suitable tool for biomedical applications where flexibility and small thickness are paramount to avoid complications. Additionally, maintaining transparency and miniaturized overall dimensions ease handling, *in vivo* aligning the implant to target a specific cortical region during the surgery.

### D. Electrochemical Impedance Spectroscopy (EIS) measurements

EIS measurements were carried out using a potentiostat (Squidstat, Admiral Instruments). The positive gold-plated brass electrode was used as the working electrode and the stainless steel ground electrode was used as the counter electrode. A silver-silver chloride electrode was used as a reference electrode. The measurement was conducted in a phosphate-buffered saline (PBS) media. A sine wave with an amplitude of 10 mV was applied and the frequency was swept between 1 MHz and 1 Hz.

### E. Craniotomy and *in vivo* implant placement

The implant was tested ( $n = 6$  rodents) using the proposed e-dura substitute stimulation method. Prior to the craniotomy, anesthesia was induced using a ketamine / xylazine (KX) cocktail with a dose of (75/10 mg/kg) through intraperitoneal (IP) injection. Anesthesia was maintained using a ketamine dose of 25 mg/kg that was administered every 45 to 60 minutes and a xylazine dose of 5 mg/kg every 2 hours. Observation of anesthesia was performed by squeezing the rat's foot pad

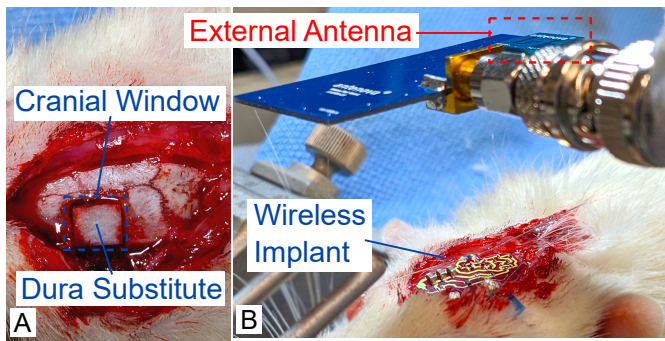


Fig. 5. *In vivo* experimental setup showing A) Craniotomy and placement of dura substitute. B) Conformal positioning of the wireless implant on the bone surface for stimulation of the motor cortex. The external antenna delivers an OOK-modulated wireless signal.

every 15 minutes. Oxygen was supplied at 2 L/minute through a nose cone. An incision was made after shaving the head using a sterile blade along the midline to expose the skull. Four 3-mm holes were drilled in a region within up to 5 mm lateral, 5 mm anterior, and 5 mm posterior of bregma, above the motor cortex. The skull was thinned around the perimeter of the cranial window using a Dremel bit and the bone was lifted using rongeurs. A piece of dura substitute with a similar size to the craniotomy was soaked in phosphate-buffered saline (PBS) and placed on the cranial window, reproducing the target clinical application wherein the device would be placed before closure after completing the neurosurgery. A picture of the placed dura substitute is shown in Fig. 5A.

The wireless implant was then positioned gently on the cranial window, with the positive electrode in contact with the dura substitute and resembling the setup shown in Fig. 1. The ground electrode was placed under the skin, and the positive measurement electrode was insulated using a small piece of wafer dicing tape. Fig. 5B shows a picture of the implant, placed conformally on the bone surface, and making contact with the dura substitute. After performing electrical stimulation and observing limb response, the animal was euthanized through an IP injection of a pentobarbital-based euthanasia solution with a dose of 100 mg/kg. At the end of each experiment, the implant was washed with a proteolytic disinfecting solution (Puremoist) and 70% isopropyl alcohol. Four identical implants were fabricated for the study, but we were able to successfully reuse the same device for testing in 6 animals, showing good durability and tolerance to handling, placement, voltage measurement, and washing.

#### F. Wireless stimulation protocol

The external transmitter that was described in Section II.A and shown in the block diagram in Fig. 2 was used to generate an RF signal at a frequency of 2.45 GHz. This signal was OOK-modulated using a function generator (33250A, Agilent) to obtain a burst of ten RF pulses each with a width of 200  $\mu$ s at a frequency of 100 Hz. The RF burst was transmitted at a frequency of 1 Hz. The parameters of the wireless stimulation protocol are shown in Fig. 6. Varying the pulse protocol is known to greatly affect the motor response threshold [39],

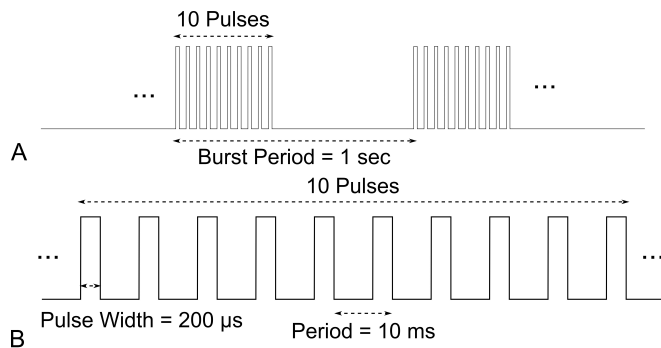


Fig. 6. The wireless stimulation protocol that was used to trigger motor response. A) A 10-pulse train is transmitted at 1 Hz. B) The parameters of an individual pulse train.

with a wide parameter space for potential exploration [40]. The transmit power was adjusted as needed until a motor response was triggered, but it was limited to 30 dBm. The external antenna with dimensions of  $10 \times 10 \text{ mm}^2$  and gain of 4.1 dBi was placed at a distance of 20 mm away from the wireless implant, as shown in Fig. 5B.

#### G. Benchtop and *in vivo* data acquisition

Voltage signals in the benchtop were measured by connecting stainless steel wires to the positive and ground electrodes on the top layer. The signals were acquired using the NI DAQExpress program. The current measurement in saline was performed by measuring the voltage drop across a series 10  $\Omega$  resistor. A PDMS chamber with a volume of  $6.9 \times 16.8 \times 10 \text{ mm}^3$  was molded using a 3D-printed master mold (form3, Formlabs), and it was used to hold saline. Coated stainless steel wires were connected from the implant to the saline chamber with 1 mm of exposed tips.

During *in vivo* experiments, the closed circuit voltage was measured by connecting mini hooks (CAB-00501, Sparkfun Electronics) to the ground electrode and the positive electrode measurement wire at the top layer while triggering limb movement. The mini hooks enable gentle contact with the measurement wires without the risk of detaching them or pulling the implant out from its position. The open circuit voltage was acquired by removing the ground electrode from under the skin and, therefore, disconnecting the animal from the implant's output, and leaving only the 10 k $\Omega$  resistor as the load. Limb deflection data was obtained by taking video recordings of the limb and using the Tracker open-source physics software to track pixel movement. A small piece of masking tape was attached to the limb to facilitate pixel tracking, and a calibration tool was used to convert the shift in pixels into limb deflection distance.

#### H. Histology

Histology was performed to assess the impact of placing the implant and electrical stimulation on tissue integrity. A bilateral craniotomy was performed in two animals prior to administering stimulation and two identical pieces of dura substitute were introduced in each animal, as shown in Supplementary Material Fig. S6. The implant's electrode made

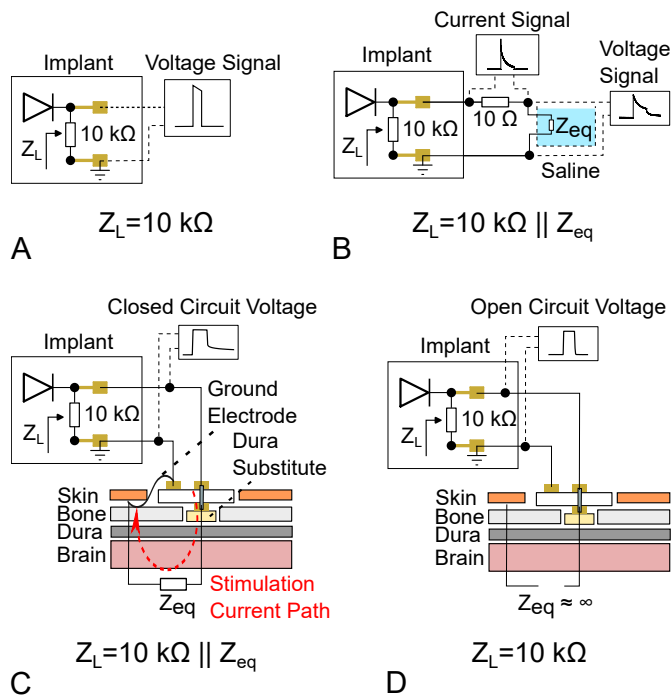


Fig. 7. Experimental setup used in the A) Benchtop test B) Saline media benchtop test C) Closed circuit and D) Open circuit voltage measurement. Each subfigure shows the load seen looking into the electrodes ( $Z_L$ ).

contact with one dura graft site (stimulation) and there was no contact with the other dura graft site (sham). The stimulation experiment was performed for at least 180 minutes. At the end of the stimulation experiment, the animal was placed in deep anesthesia by a ketamine-xylazine injection. The heart was exposed and a small cut was made in the left ventricle. A perfusion needle (15 ga) was inserted through the ventricle until it entered the aorta. A large incision was made in the right atrium to allow the blood to flow and drain. 200 mL of PBS was delivered followed by 200 mL of 4% paraformaldehyde. The flow was maintained at 20 mL/min. Rat brains used for H&E staining were embedded in paraffin wax following fixation and sectioned into 5  $\mu\text{m}$  slices. Histology images were viewed with an Olympus BX46 microscope and selected images were captured using Standard Olympus cellSens imaging system. Whole brain slices were photographed at 12.5X and focus of ischemia at 100X.

### I. Survey

A survey was conducted at the Mayo Clinic to evaluate whether the proposed current design would represent a significant improvement over currently available medical implants capable of stimulation or recording of the neuroaxis. Only senior attendings not involved in the study who either placed medical implants or evaluated patients with medical implants were eligible for the survey.

## III. RESULTS

### A. Wireless implant benchtop characterization

The implant's output voltage was assessed in the benchtop as a function of external transmitted power, distance, and OOK

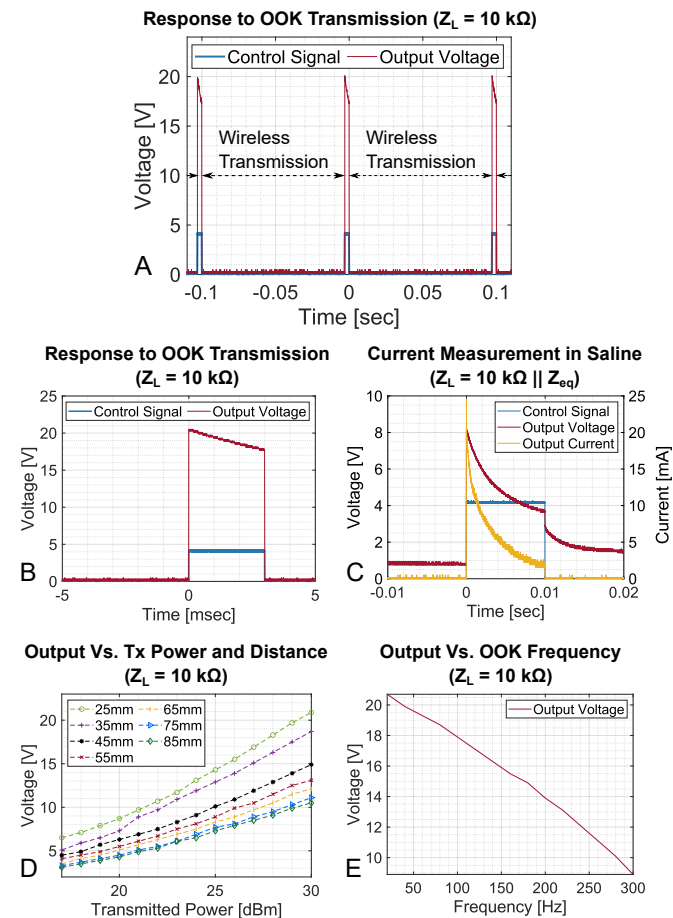


Fig. 8. Benchtop characterization of the wireless implant in various conditions. A) The implant responds to OOK transmission by generating monophasic voltage pulses. B) A higher resolution view of a single pulse similar pulse width to the OOK control signal. C) Voltage and current waveforms delivered in a saline solution. D) Amplitude of monophasic voltage pulses as a function of RF transmit power and distance to the external antenna. E) Output voltage as a function of OOK signal frequency.

modulation frequency. A diagram of the benchtop test is shown in Fig. 7.A and B. The load seen looking into the electrodes ( $Z_L$ ) is equal to  $R3$  with a value of 10 k $\Omega$ . All benchtop tests were conducted at an RF frequency of 2.45 GHz and without voltage regulation implemented at the output. The implant generates monophasic voltage pulses in response to OOK modulation of the RF carrier with negligible delay as shown in Fig. 8A and Fig. 8B which provides a higher resolution capture of an individual monophasic pulse that is delivered to a 10 k $\Omega$  load. A discharging effect can be clearly observed when the pulse width is 3 ms and its rate is determined by the time constant formed by the storage capacitor ( $C9$ ) and the load at the electrodes. This discharge effect can be eliminated by increasing the value of the storage capacitor; however, in this work, the stimulation protocol comprises pulses with a width of 200  $\mu\text{s}$  with a negligible discharge when using a 30  $\mu\text{F}$  storage capacitor as shown in Section III.C.

When performing a similar test in saline, a discharge effect can be clearly observed in Fig. 8C due to the highly capacitive nature of the saline media. In this measurement, the load seen looking into the electrodes is  $Z_L = R3 \parallel Z_{eq}$  where

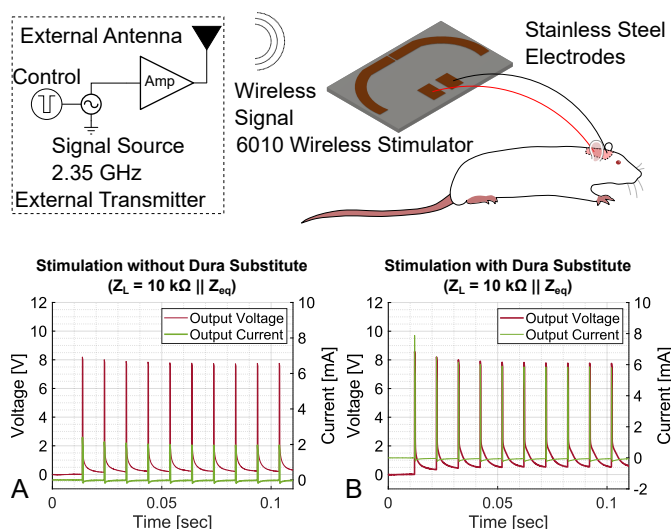


Fig. 9. A comparison of voltage and current requirements for triggering hindlimb response between the proposed stimulation method through the dura substitute and conventional direct epidural stimulation. Top: *In vivo* experimental setup. A) Closed circuit voltage and current waveforms without dura substitute. B) Closed circuit voltage and current using dura substitute.

$Z_{eq}$  is the equivalent impedance of the saline media. The implant delivers several milliamps of current in saline, within the typical range for cortical stimulation applications. Further electrode characterization results that were obtained using EIS measurements are shown in Supplementary Material Fig. S7.

The output voltage was measured as a function of distance and external transmitted power as shown in Fig. 8D. Each marker in the figure represents a measurement point. The implant generates up to 21 V at the maximum transmit power (30 dBm) and a distance of 25 mm to the external antenna in an air medium. The output voltage decreases as the external antenna is moved away from the implant, and the impact of increasing distance on the output voltage becomes less significant as the antenna is moved out towards the far-field region. The output voltage is also impacted by the OOK frequency at any given transmit power and distance. For any stimulation frequency below 20 Hz, the energy storage capacitors have adequate time to fully charge. However, as the frequency is increased to 300 Hz, the output voltage drops by around 50% due to insufficient charging time.

For future chronic applications, it is beneficial to convert the monophasic voltage pulses into biphasic, charge-balanced pulses in order to prolong the electrodes' lifetime and avoid hydrolysis. An implementation of a charge balancing circuit, composed of a series capacitor and a shunt resistor that approximates the real impedance of tissue in parallel with the 10 k $\Omega$  resistor is shown in Supplementary Material Fig. S8.

### B. Comparison between dura substitute and conventional epidural stimulation

Before testing the proposed wireless implant, a preliminary study was conducted to determine and compare the voltage and current for triggering limb movement using the proposed e-dura substitute method versus the conventional direct epidural

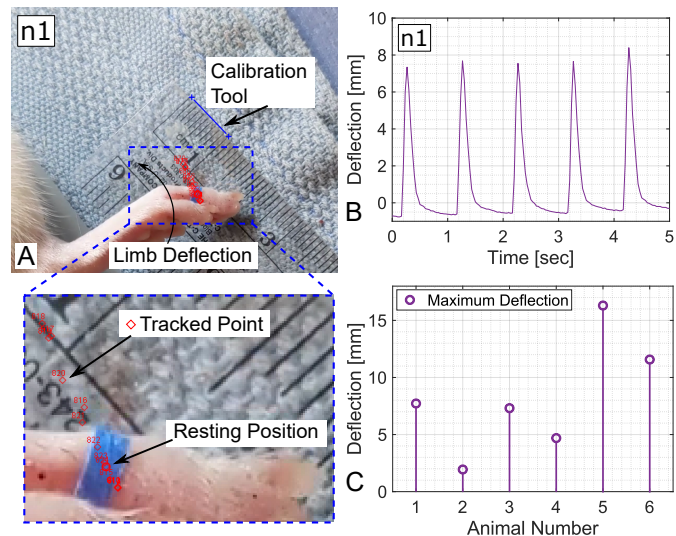


Fig. 10. Limb deflection recordings resulting from wireless electrical stimulation using the dura substitute. A) Limb deflection was found by measuring the total distance traveled from the resting position. Inset: Closer view showing several tracked points and resting position B) A plot of limb deflection from one animal. C) Peak deflection averaged over 5 stimulation bursts recorded in  $n = 6$  animals.

stimulation method, in the absence of a dura substitute. In this experiment, a wireless stimulator that we designed and fabricated on a Rogers 6010 substrate (referred to as 6010 stimulator) was used [38]. The stimulator has a similar circuit structure as the proposed wireless implant, and it is equipped with energy storage capacitors with an identical value (30  $\mu$ F). The 6010 stimulator can therefore be used to gain useful insights into the voltage and current requirements for e-dura stimulation. Two stainless steel electrodes were connected to the 6010 stimulator as shown in Fig. 9. They were gently placed on the cortical surface and then on the dura substitute using micro-manipulators, and used to deliver electrical stimulation in these two distinct conditions. The external transmitter was placed at a distance of 30 mm away from the 6010 stimulator.

The results show that both methods can be used to trigger limb motor response. The current required in conventional stimulation is around 2 mA, as shown in Fig. 9A. A larger current is needed to trigger a motor response when using the e-dura substitute method, and it was found to be around 6 mA, as shown in Fig. 9B. The dura substitute creates a low-resistance non-stimulation path, allowing a greater proportion of the stimulation electrode current to return to the ground electrode through the dura substitute without entering into cortex (see Fig. 7.C). Therefore, the effective strength of the current is reduced and a larger total current is needed to stimulate the motor neurons. This experiment shows that it is possible to perform stimulation using the proposed e-dura substitute method, with a decreased efficiency by around 60% due to current loss, but with the same reliability as the conventional stimulation method. At least 30 seconds of recordings were taken using these two approaches at a stimulation frequency of 1 Hz, with negligible delay in motor response and impact on limb deflection when using the e-dura substitute method.

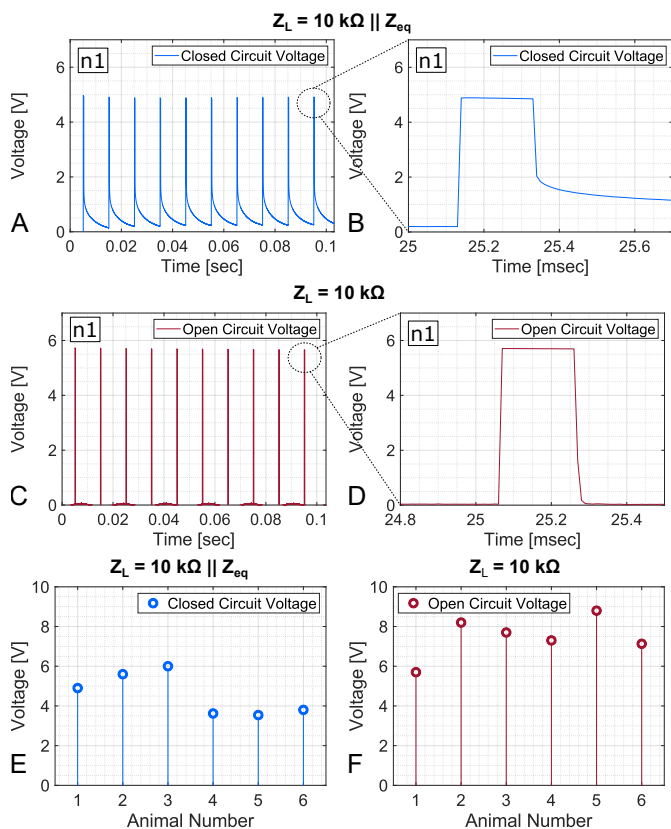


Fig. 11. *In vivo* open circuit and closed circuit voltage recordings of wireless stimulation using the dura substitute. A) A capture of a closed circuit stimulation burst and B) a higher resolution view of a single monophasic voltage pulse. C) A capture of an open circuit stimulation burst and D) a higher resolution view of a single monophasic voltage pulse. E) Peak closed circuit and F) open circuit voltage recorded in  $n = 6$  animals.

### C. Wireless stimulation using the e-dura substitute method

Wireless stimulation triggered a motor response in all rat models ( $n = 6$ ) and the movement correlated with the stimulation frequency of 1 Hz during the entire recording period of 30 seconds in each animal. Limb deflection (total distance from resting limb position, Fig. 10A) was recorded for at least 30 seconds for all rat models. A capture with a period of 5 seconds showing limb deflection in animal  $n1$  is plotted in Fig. 10B. The distinctive peaks were observed when wireless stimulation was delivered at 1 Hz, and no deflection was observed in the absence of wireless transmission. Captures of limb deflection in the rest of the animals are shown in Supplementary Material Fig. S9, showing similar characteristics and distinct peaks at 1 Hz. The peak limb deflection, averaged over a 5-second period is plotted for all animals in Fig. 10C. The average limb deflection measured in 6 animals was found to be  $8.2 \pm 5.3$  mm with 99% confidence level. This deflection corresponds to stimulation just above the motor neuron threshold. Further increasing the transmitted power was observed to increase the limb deflection. Note that the required stimulation current and the resulting limb deflection depend on many additional factors: the animal's anesthesia depth, any acute surgical injuries, and the exact position of the electrodes on the motor cortex can all cause substantial variations.

The closed circuit voltage that is required to trigger motor

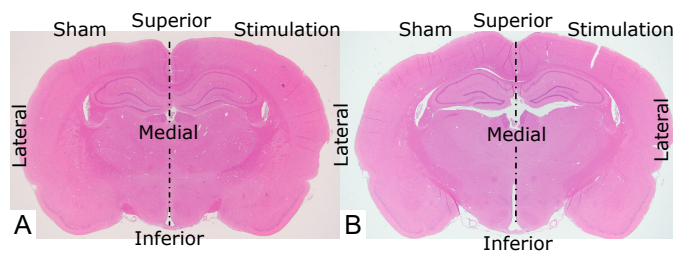


Fig. 12. Histology of rat brain sections after stimulation using the dura substitute. (A, B) Coronal cut sections with H&E staining at 12.5X illustrating two different animals submitted to bilateral craniotomies for placement of implant without stimulation (sham) and implant with stimulation (stimulation). A histopathological review of both slides revealed intact tissue architecture in both hemispheres.

response was recorded while measuring limb movement. The experimental setup for measuring the closed-circuit voltage is shown in Fig. 7.C. The ground electrode is placed under the skin, creating a stimulation current path that is delivered through the dura substitute. Therefore, the load seen looking into the electrodes is  $Z_L = R3 \parallel Z_{eq}$  where  $Z_{eq}$  is the equivalent impedance of the stimulation current path. The closed circuit measurement is shown in Fig. 11A for a period lasting a full burst and in Fig. 11B which provides a higher resolution capture of a single monophasic voltage pulse for animal  $n1$ . Similar to current measurements in saline media, the voltage pulses exhibit a discharge effect when testing *in vivo*.

The open circuit voltage was found by disconnecting the ground electrode while maintaining the implant's placement and distance to the external antenna and keeping the RF transmit power and stimulation parameters unchanged. The experimental setup for measuring the open circuit voltage is shown in Fig. 7.D. By removing the ground electrode, the stimulation current path is open and its equivalent impedance is  $Z_{eq} \approx \infty$  and the load looking into the electrodes is  $Z_L = 10$  k $\Omega$ . A recording of the open circuit voltage is shown in Fig. 11C and D.

The peak closed circuit and open circuit voltage are taken for  $n = 6$  animals and are shown in Fig. 11E and F, respectively. The average closed circuit voltage is  $4.57 \pm 1.13$  V with 99% confidence level. Comparing the closed circuit voltage with the current measurements in Fig. 9 allows us to approximate the value of  $Z_L = R3 \parallel Z_{eq}$  which is the equivalent impedance of the stimulation current path in parallel with the 10 k $\Omega$  load resistor at 2 k $\Omega$ . These results show good consistency with the data provided in [34] where the impedance magnitude of a collagen solution was found to range between 1 k $\Omega$  and 3 k $\Omega$  at a frequency of 100 Hz, depending on the concentration of collagen in the solution. This estimation is useful when determining the value of the series capacitor that is used for charge balancing when testing the implant in a chronic setting. The average open circuit voltage is  $7.47 \pm 1.11$  V with a confidence level of 99%.

### D. Histology

A review of consecutive histological slides in 2 rats revealed intact tissue architecture without relevant anomalies in both

sham- and stimulated-hemispheres (Fig. 12). A small region of acute ischemic injury with neuropil vacuolation and red neurons was found in a single slice on the sham-hemisphere (Supplementary Material Fig. S10), representing a potential iatrogenic artifact induced by surgical manipulation.

#### E. Survey

A total of 7 faculty members who have ample experience with implant placement or evaluation of patients with medical implants were included. Out of the surveyed faculty members, 86% strongly agreed that the device would represent a significant improvement over currently available models and that they would use the device if clinically available. The dura-based embodiment was also considered a significant advance with 71% of the surveyed faculty either agreeing or strongly agreeing with that statement, and 71% of the surveyed faculty either agreeing or strongly agreeing that they were satisfied with the current design of the device.

### IV. DISCUSSION

This study demonstrates the efficacy of the e-dura substitute method as a potential approach that allows supplementing neuromodulation with the potential advantage of a higher safety profile and reduced risk of bleeding, infection, and wire migration. Histological analysis of sacrificed rat brains illustrates the absence of tissue architecture changes with acute stimulation when compared with sham-implant, suggesting the safety of tested materials and methodologies in acute settings. Future studies with chronic stimulation would be needed to evaluate for potential long-term iatrogenic injury. The *in vivo* testing results revealed insights into the voltage required for effective motor stimulation and provided a comparison with the efficiency of the conventional cortical stimulation method. The measured open circuit voltage was smaller *in vivo* when compared to the benchtop measurements at a given transmit power and distance to the external antenna. This reduction can be attributed to the higher relative dielectric constant of the surrounding tissue. In addition, the metallic surgical equipment, such as micro-manipulators, ear bars, and tweezers disturb the wireless signal in the vicinity of the implant. The measured open circuit and closed circuit voltage showed good agreement across all animals. The observed voltage variations are caused by several factors, such as the positioning of the ground electrode or variations in the impedance seen by the implant due to variations in the amount of saline present within and around the dura substitute. In future long-term tests, the implant will be placed under the skin, leading to higher attenuation in the power received by the implant. To mimic the impact of skin suturing, we covered the implant (including the antenna) with surgical tissue that was soaked in saline, and we were able to trigger a motor response by decreasing the distance to the external antenna to 10 mm and setting the transmit power to 30 dBm. The antenna length or the matching inductor may be tuned in chronic applications, and a voltage regulation circuit, composed of a series resistor and a shunt Zener diode will be added without any significant increase in substrate size. The peak limb deflection was proportional to the

closed circuit voltage, however, the positioning of the implant had a significant impact on the peak deflection. A smaller peak deflection was observed in *n*2 because the implant was not well aligned above the motor cortex. Additional factors that may influence the maximum measured peak include the location of the tape on the paw that is used in tracking pixels and the anesthesia depth.

To ensure the safety of using the proposed wireless implant, the Specific Absorption Rate (SAR) must be considered when selecting the RF frequency of operation in long-term studies and human implementations. SAR increases with higher frequencies [42]; therefore, the implant may be realized using a different RF frequency by varying the length of the dipole antenna and ensuring minimum SAR depending on the electrical properties of human tissue. Owing to the larger human anatomy, the dipole antenna can be designed at a lower frequency to reduce SAR, and the methodology used in this work can be followed to find the optimal inductor value at a different frequency using harmonic balance simulations and experimental verification.

Table I shows a comparison between the wireless implant proposed in this work and similar wireless implants reported in the literature, with a focus on implants used for stimulation. The most distinctive feature of this work is that it is the only study where wireless electrical stimulation was delivered without contact between electrodes and the target organ, through an FDA-approved dura substitute. Various crucial parameters are listed, such as the frequency of the transmitted wireless signal, maximum transmit power, and output voltage. When examining the output voltage, some studies report the regulated output voltage, but the device can generate even higher voltage values without regulation in the benchtop [18], [41]. Although the proposed implant can generate up to 21 V when transmission occurs in an air medium, we report the closed circuit voltage, averaged over 6 animals, in this comparison table.

The table lists the materials that are used to make the main substrate on top of which the electronics are assembled. Polyimide [19], [26], [41] is commonly used as a substrate due to several attractive features including durability, flexibility, and biocompatibility. While PDMS has been used as an encapsulation material [18], [26] to shield the main substrate through dip coating, this work presents the only design where PDMS is used as the main substrate. Contrary to relying on a non-biocompatible conductor such as copper [18], [26], [41] to interconnect the implant circuit, we deposited gold, a biocompatible and malleable metal, directly on the Parylene/PDMS substrate. Therefore, the proposed implant is the only one that utilizes a flexible and transparent substrate.

When reporting the substrate size, we accounted for the total substrate area on top of which the main components (diodes, capacitors, microcontroller) are placed. We excluded electrodes from the substrate size because their dimensions and shape depend on the application. For example, deep brain electrodes or cardiac electrodes are typically larger than cortical stimulation electrodes. The circuitry of the proposed implant occupies an area of 103 mm<sup>2</sup> and it is almost equal in area to the devices reported in [14], [26]. The only device

TABLE I  
STATE-OF-THE-ART COMPARISON

Ref	Tx Freq. (GHz)	Substrate Material	Flexible /Transparent Substrate?	Output Voltage (V)	Tx-Rx Distance (mm)	Max. Tx Power (dBm)	Tech	Peak Thickness (mm)	Substrate (mm <sup>3</sup> )	Size	Tx (mm <sup>2</sup> )	Size
<b>This*</b>	2.45	Parylene/PDMS	Yes/Yes	4.57	20	30	Discrete	0.61	15.6 × 6.6 × 0.11		10 × 10	
[14]	1.2	Rogers TMM	No/No	< 1.8	25	10	Discrete	2.42	10 × 10 × 1.52 <sup>a</sup>		230 × 140	
[15]	2.4	soft elastomer	Yes/No	1	10	22.6	Discrete	3	15 × 2.7 <sup>b</sup>		π × 184.9	
[17]	2.4	polyester	No/No	3	15	20.49	Discrete	7	22 × 23 × 7		59 × 88	
[18]	0.013	Multiple <sup>c</sup>	Yes/No	5.5	Variable <sup>d</sup>	34.77	Discrete	0.92 <sup>e</sup>	22 × 8 × 0.17		280 × 220	
[19]	345e <sup>-6</sup>	Multiple <sup>f</sup>	No/No	3.3	35	30	CMOS	14.8	3 × 2.15 × 14.8		π × 1225	
[26]	0.013	polyimide	Yes/No	2.2	Variable <sup>g</sup>	39	Discrete	0.874 <sup>h</sup>	π × 31.36 × 0.124		140 × 250	
[41]	0.013	polyimide	Yes/No	5.6	Variable <sup>i</sup>	39	Discrete	0.928 <sup>j</sup>	π × 49 × 0.128		220 × 220	

\* **The only study where electrical stimulation was delivered without direct contact between the electrodes and the target organ.** <sup>a</sup> Used an enclosure with thickness of 4.5 mm. <sup>b</sup> The design is tube-shaped (length×diameter). <sup>c</sup> Multiple materials are used, but the thickest layer is polyimide. <sup>d</sup> The study was conducted on moving animals in a 28 × 22 cm<sup>2</sup> cage. <sup>e</sup> An additional increase beyond this peak is caused by PDMS encapsulation layer. <sup>f</sup> The device consists of a magneto electric film and a CMOS chip encapsulated in epoxy. <sup>g</sup> The study was conducted on moving animals. <sup>h</sup> An additional increase beyond this peak is caused by PDMS encapsulation layer. <sup>i</sup> The study was conducted on moving animals. <sup>j</sup> An additional increase beyond this peak is caused by parylene encapsulation layer.

with a smaller area in the comparison table is reported in [19] which is fabricated using a CMOS process. CMOS fabrication results in a significantly smaller footprint compared to using discrete components, at an increased fabrication cost. The proposed implant achieves the smallest substrate thickness at 0.11 mm and this value takes into consideration the main PDMS substrate and the two Parylene layers (interface and passivation). While the studies reported in [26], [41] report a similar substrate thickness compared to our work, it is important to highlight that these implants were dip-coated in PDMS after assembly, leading to an increase in substrate thickness that is not directly reported. In addition to the substrate thickness, the table also reports the peak thickness for various designs. The integration of electronics with various sizes generates a surface topology as shown in Supplementary Material Fig. S4J. The storage capacitors used in this work have the largest thickness which is determined by voltage rating. When using GRM-series capacitors from Murata with a voltage rating of 10 V, the proposed implant achieves a peak thickness of 0.61 mm which is the thinnest in the comparison table. This work also uses the smallest external antenna compared to other studies where the distance to the implant is fixed. We achieved this by transmitting the wireless signal at a higher frequency compared to the majority of studies reported in the table. However, it is important that several studies were conducted on moving animals where a loop antenna with equal dimensions to the cage was used [18], [26], [41] and a higher transmit power was needed compared to our work to provide adequate coverage throughout the cage volume.

The answers to the survey are shown in Table II, and they illustrated the interest of surgeons and epileptologists in the introduction to clinical practice of a device with the capabilities evaluated in this study. Interestingly, surveyed faculty members offered suggestions for new versions to suit their particular medical practices, including the design of smaller implants capable of being deployed for spinal cord stimulation or the application of the device on spinal cord stimulator paddles already in use. While most surveyed faculty members agreed that the device could lead to improved patient outcomes, consensus favored the need for subsequent studies demonstrating long-term safety.

## V. CONCLUSION

This paper presented the design, fabrication, and *in vivo* testing of a wireless, battery-free implant for cortical brain stimulation. The device can be externally controlled to generate any required stimulation protocol by using an OOK-modulated wireless signal. Before this work, PDMS and Parylene were commonly used as coating materials to shield the implant from surrounding tissue. However, we showed that direct fabrication of electronics on PDMS with a Parylene adhesion layer allows us to achieve ultra-small substrate thickness, flexibility, and transparency. The implant showed good durability by acute testing in 6 animals. We introduced the e-dura substitute as a reliable platform that enables reconstruction and appropriate surgical closure with an embedded platform for neuromodulation. This approach can drastically improve the risk-reward ratio by targeting applications towards low-risk placement during already-occurring brain and spine

TABLE II  
SURVEY ANSWERS OF HEALTH CARE PROFESSIONALS INCLUDING SURGEONS AND EPILEPTOLOGISTS (N=7)

Survey Question	Strongly Disagree %	Disagree %	Neither %	Agree %	Strongly Agree %
<i>This device would represent a significant improvement over currently available models.</i>	0	0	0	14	86
<i>I would use this device if available for commercial use.</i>	0	0	0	14	86
<i>This device would lead to improved patient outcomes.</i>	0	0	43	29	29
<i>This novel surgical embodiment, using an off-the-shelf dural graft represents a significant improvement over currently available techniques.</i>	0	0	29	57	14
<i>I have experience with the placement of stimulators or recording capable medical implants.</i>	0	0	0	0	100
<i>I am satisfied overall with the current design of the device and its applicability.</i>	0	0	29	29	43

surgeries. A possible future direction of this work may include investigating the long-term performance of the implant by conducting chronic experiments on moving rat models and/or larger animal models.

#### ACKNOWLEDGMENT

Research reported in this publication was supported by HHS-NIH: National Institute of Biomedical Imaging and Bioengineering (NIBIB) of the National Institutes of Health under award number R21 EB028396 and 2022 Mayo Clinic and Arizona State University Alliance for Health Care Collaborative Research Seed Grant Program. The animal work was performed under Arizona State University IACUC (Institutional Animal Care and Use Committee) approved protocol 21-1822R in compliance with all university guidelines and regulations. The authors would like to acknowledge Dr. Reed Bjorklund, ASU, and Dr. Mark Edgar, Mayo Clinic, for helping with animal perfusion and histology. A.Q.-H. acknowledges the support from the William J. and Charles H. Mayo Professorship, the Mayo Clinic Clinician Investigator Award, the Florida Department of Health Cancer Research Chair Fund, and the Monica Flynn Jacoby Endowed Chair.

#### REFERENCES

[1] S. Huang, Y. Liu, Y. Zhao, Z. Ren, and C. F. Guo, "Flexible electronics: stretchable electrodes and their future," *Advanced Functional Materials*, vol. 29, no. 6, p. 1805924, 2019.

[2] J. Shi and Y. Fang, "Flexible and implantable microelectrodes for chronically stable neural interfaces," *Advanced Materials*, vol. 31, no. 45, p. 1804895, 2019.

[3] Y. Cho, S. Park, J. Lee, and K. J. Yu, "Emerging materials and technologies with applications in flexible neural implants: a comprehensive review of current issues with neural devices," *Advanced Materials*, vol. 33, no. 47, p. 2005786, 2021.

[4] P. A. Rivera-Rivera, M. Rios-Lago, S. Sanchez-Casarrubios, O. Salazar, M. Yus, M. González-Hidalgo, A. Sanz, J. Avecillas-Chasin, J. Alvarez-Linera, A. Pascual-Leone, *et al.*, "Cortical plasticity catalyzed by prehabilitation enables extensive resection of brain tumors in eloquent areas," *Journal of Neurosurgery*, vol. 126, no. 4, pp. 1323–1333, 2017.

[5] A. J. Fenoy and R. K. Simpson, "Risks of common complications in deep brain stimulation surgery: management and avoidance," *Journal of neurosurgery*, vol. 120, no. 1, pp. 132–139, 2014.

[6] S. Bjercknes, I. M. Skogseid, T. Sæhle, E. Dietrichs, and M. Toft, "Surgical site infections after deep brain stimulation surgery: frequency, characteristics and management in a 10-year period," *PloS one*, vol. 9, no. 8, p. e105288, 2014.

[7] O. Jitkrisadakul, R. Bhidayasiri, S. K. Kalia, M. Hodaie, A. M. Lozano, and A. Fasano, "Systematic review of hardware-related complications of deep brain stimulation: do new indications pose an increased risk?," *Brain Stimulation*, vol. 10, no. 5, pp. 967–976, 2017.

[8] R. E. Kirkfeldt, J. B. Johansen, E. A. Nohr, O. D. Jørgensen, and J. C. Nielsen, "Complications after cardiac implantable electronic device implantations: an analysis of a complete, nationwide cohort in Denmark," *European heart journal*, vol. 35, no. 18, pp. 1186–1194, 2014.

[9] G. L. Barbruni, P. M. Ros, D. Demarchi, S. Carrara, and D. Ghezzi, "Miniaturised wireless power transfer systems for neurostimulation: A review," *IEEE Transactions on Biomedical Circuits and Systems*, vol. 14, no. 6, pp. 1160–1178, 2020.

[10] S. Rao and J.-C. Chiao, "Body electric: Wireless power transfer for implant applications," *IEEE Microwave Magazine*, vol. 16, no. 2, pp. 54–64, 2015.

[11] S. A. Mirbozorgi, P. Yeon, and M. Ghovanloo, "Robust wireless power transmission to mm-sized free-floating distributed implants," *IEEE transactions on biomedical circuits and systems*, vol. 11, no. 3, pp. 692–702, 2017.

[12] C.-L. Yang, C.-K. Chang, S.-Y. Lee, S.-J. Chang, and L.-Y. Chiou, "Efficient four-coil wireless power transfer for deep brain stimulation," *IEEE Transactions on Microwave Theory and Techniques*, vol. 65, no. 7, pp. 2496–2507, 2017.

[13] D. K. Freeman, J. M. O'Brien, P. Kumar, B. Daniels, R. A. Irion, L. Shraytah, B. K. Ingersoll, A. P. Magyar, A. Czarnecki, J. Wheeler, *et al.*, "A sub-millimeter, inductively powered neural stimulator," *Frontiers in neuroscience*, vol. 11, p. 659, 2017.

[14] S. M. Asif, J. Hansen, M. S. Khan, S. D. Walden, M. O. Jensen, B. D. Braaten, and D. L. Ewert, "Design and in vivo test of a batteryless and fully wireless implantable asynchronous pacing system," *IEEE Transactions on Biomedical Engineering*, vol. 63, no. 5, pp. 1070–1081, 2015.

[15] Y. Tanabe, J. S. Ho, J. Liu, S.-Y. Liao, Z. Zhen, S. Hsu, C. Shuto, Z.-Y. Zhu, A. Ma, C. Vassos, *et al.*, "High-performance wireless powering for peripheral nerve neuromodulation systems," *PLoS One*, vol. 12, no. 10, p. e0186698, 2017.

[16] A. Khalifa, Y. Karimi, Q. Wang, W. Montlouis, S. Garikapati, M. Stanačević, N. Thakor, and R. Etienne-Cummings, "The microbead: A highly miniaturized wirelessly powered implantable neural stimulating system," *IEEE transactions on biomedical circuits and systems*, vol. 12, no. 3, pp. 521–531, 2018.

[17] Q. Xu, D. Hu, B. Duan, and J. He, "A fully implantable stimulator with wireless power and data transmission for experimental investigation of epidural spinal cord stimulation," *IEEE Transactions on Neural Systems and Rehabilitation Engineering*, vol. 23, no. 4, pp. 683–692, 2015.

[18] A. Burton, S. M. Won, A. K. Sohrabi, T. Stuart, A. Amirhossein, J. U. Kim, Y. Park, A. Gabros, J. A. Rogers, F. Vitale, *et al.*, "Wireless, battery-free, and fully implantable electrical neurostimulation in freely

- moving rodents,” *Microsystems & Nanoengineering*, vol. 7, no. 1, p. 62, 2021.
- [19] J. C. Chen, P. Kan, Z. Yu, F. Alrashdan, R. Garcia, A. Singer, C. E. Lai, B. Avants, S. Crosby, Z. Li, *et al.*, “A wireless millimetric magnetoelectric implant for the endovascular stimulation of peripheral nerves,” *Nature Biomedical Engineering*, vol. 6, no. 6, pp. 706–716, 2022.
- [20] H. Lyu, J. Wang, J.-H. La, J. M. Chung, and A. Babakhani, “An energy-efficient wirelessly powered millimeter-scale neurostimulator implant based on systematic codesign of an inductive loop antenna and a custom rectifier,” *IEEE transactions on biomedical circuits and systems*, vol. 12, no. 5, pp. 1131–1143, 2018.
- [21] M. Vallejo, J. Recas, P. G. Del Valle, and J. L. Ayala, “Accurate human tissue characterization for energy-efficient wireless on-body communications,” *Sensors*, vol. 13, no. 6, pp. 7546–7569, 2013.
- [22] Y. S. Choi, R. T. Yin, A. Pfenniger, J. Koo, R. Avila, K. Benjamin Lee, S. W. Chen, G. Lee, G. Li, Y. Qiao, *et al.*, “Fully implantable and bioresorbable cardiac pacemakers without leads or batteries,” *Nature biotechnology*, vol. 39, no. 10, pp. 1228–1238, 2021.
- [23] K.-Y. Yeh, H.-W. Chiu, W.-T. Tseng, H.-C. Chen, C.-T. Yen, S.-S. Lu, and M.-L. Lin, “A Dual-Mode Multifunctional Pulsed Radio-Frequency Stimulator for Trigeminal Neuralgia Relief and its Animal Model,” *IEEE Transactions on Biomedical Circuits and Systems*, vol. 15, no. 4, pp. 719–730, 2021.
- [24] D. K. Biswas and I. Mahbub, “A 0.09 mm<sup>2</sup> On-Chip Wireless Power Transfer System Designed in 0.5  $\mu$ m CMOS Process for Brain Neuro-modulation Applications,” *IEEE Journal of Electromagnetics, RF and Microwaves in Medicine and Biology*, vol. 4, no. 2, pp. 117–125, 2020.
- [25] A. Iqbal, M. Al-Hasan, I. B. Mabrouk, A. Basir, M. Nedil, and H. Yoo, “Biotelemetry and wireless powering of biomedical implants using a rectifier integrated self-diplexing implantable antenna,” *IEEE Transactions on Microwave Theory and Techniques*, vol. 69, no. 7, pp. 3438–3451, 2021.
- [26] P. Gutruf, R. T. Yin, K. B. Lee, J. Ausra, J. A. Brennan, Y. Qiao, Z. Xie, R. Peralta, O. Talarico, A. Murillo, *et al.*, “Wireless, battery-free, fully implantable multimodal and multisite pacemakers for applications in small animal models,” *Nature communications*, vol. 10, no. 1, p. 5742, 2019.
- [27] C. P. Constantin, M. Aflori, R. F. Damian, and R. D. Rusu, “Biocompatibility of polyimides: A mini-review,” *Materials*, vol. 12, no. 19, p. 3166, 2019.
- [28] J. Charthad, T. C. Chang, Z. Liu, A. Sawaby, M. J. Weber, S. Baker, F. Gore, S. A. Felt, and A. Arbabian, “A mm-sized wireless implantable device for electrical stimulation of peripheral nerves,” *IEEE transactions on biomedical circuits and systems*, vol. 12, no. 2, pp. 257–270, 2018.
- [29] P. K. Sharma, N. Gupta, and P. I. Dankov, “Characterization of polydimethylsiloxane (PDMS) as a wearable antenna substrate using resonance and planar structure methods,” *AEU-International Journal of Electronics and Communications*, vol. 127, p. 153455, 2020.
- [30] R. B. Simorangkir, Y. Yang, L. Matekovits, and K. P. Esselle, “Dual-band dual-mode textile antenna on PDMS substrate for body-centric communications,” *IEEE Antennas and Wireless Propagation Letters*, vol. 16, pp. 677–680, 2016.
- [31] S. Kim, I. Towfeeq, Y. Dong, S. Gorman, A. M. Rao, and G. Koley, “P (VDF-TrFE) film on PDMS substrate for energy harvesting applications,” *Applied Sciences*, vol. 8, no. 2, p. 213, 2018.
- [32] W. Liu, X. Wang, J. Su, Q. Jiang, J. Wang, Y. Xu, Y. Zheng, Z. Zhong, and H. Lin, “In vivo Evaluation of Fibrous Collagen Dura Substitutes,” *Frontiers in Bioengineering and Biotechnology*, vol. 9, p. 628129, 2021.
- [33] *Guidance Document for Dura Substitute Devices- Guidance for Industry, U.S. Food and Drug Administration*. [Online]. Available: <https://www.fda.gov/regulatory-information/search-fda-guidance-documents/guidance-document-dura-substitute-devices-guidance-industry> (Last Accessed: October 2023).
- [34] M. Ashoorirad, M. Saviz, and A. Fallah, “On the electrical properties of collagen macromolecule solutions: Role of collagen-water interactions,” *Journal of Molecular Liquids*, vol. 300, p. 112344, 2020.
- [35] *Operation within the bands 902-928 MHz, 2400-2483.5 MHz, and 5725-5850 MHz, Title 47 Chapter I Subchapter A Part 15 C.F.R § 15.247*. [Online]. Available: <https://www.ecfr.gov/current/title-47/chapter-I/subchapter-A/part-15/subpart-C/subject-group-ECFR2f2e5828339709e/section-15.247> (Last Accessed: October 2023).
- [36] J. M. Bronstein, M. Tagliati, C. McIntyre, R. Chen, T. Cheung, E. L. Hargreaves, Z. Israel, M. Moffitt, E. B. Montgomery, P. Stypulkowski, J. Shils, T. Denison, J. Vitek, J. Volkman, J. Wertheimer, and M. S. Okun, “The rationale driving the evolution of deep brain stimulation to constant-current devices,” *Neuromodulation: Technology at the Neural Interface*, vol. 18, no. 2, pp. 85–89, 2015.
- [37] J. Volkmann, J. Herzog, F. Kopper, and G. Deuschl, “Introduction to the programming of deep brain stimulators,” *Movement Disorders*, vol. 17, no. S3, pp. S181–S187, 2002.
- [38] A. A. Benbuk, H. Esmaeili, S. Liu, A. Patino-Guerrero, R. Q. Migrino, J. Chae, M. Nikkhah, and J. Blain Christen, “Passive and Flexible Wireless Electronics Fabricated on Parylene/PDMS Substrate for Stimulation of Human Stem Cell-Derived Cardiomyocytes,” *ACS sensors*, vol. 7, no. 11, pp. 3287–3297, 2022.
- [39] H. Asanuma, A. Arnold, and P. Zarzecki, “Further study on the excitation of pyramidal tract cells by intracortical microstimulation,” *Experimental Brain Research*, vol. 26, no. 5, pp. 443–461, 1976.
- [40] W. M. Grill, “Temporal pattern of electrical stimulation is a new dimension of therapeutic innovation,” *Current Opinion in Biomedical Engineering*, vol. 8, pp. 1–6, 2018. Neural Engineering/ Novel Biomedical Technologies: Neuromodulation.
- [41] J. Ausra, M. Madrid, R. T. Yin, J. Hanna, S. Arnott, J. A. Brennan, R. Peralta, D. Clausen, J. A. Bakall, I. R. Efimov, *et al.*, “Wireless, fully implantable cardiac stimulation and recording with on-device computation for closed-loop pacing and defibrillation,” *Science advances*, vol. 8, no. 43, p. eabq7469, 2022.
- [42] D. He and Z. Chen, “Study on the Specific Absorption Rate of Implantable Medical Devices in Multilayer Tissues,” in *2022 IEEE 9th International Symposium on Microwave, Antenna, Propagation and EMC Technologies for Wireless Communications (MAPE)*, pp. 319–322, IEEE, 2022.



**Abed Benbuk** (Graduate Student Member, IEEE) received a MEng from the Department of Electrical and Computer Engineering at the American University of Beirut, Lebanon in 2020, and is currently a Ph.D. candidate at the Department of Electrical, Computer, and Energy Engineering, Arizona State University (ASU), Tempe, Arizona, USA. He joined Timing Systems and Silicon Development, Skyworks Solutions, Inc, Austin, Texas, USA, as a systems engineering intern during summer 2022 and 2023. He is currently a Research Associate at the BioElectrical Systems lab at ASU, and his research interests include RF energy harvesting and wireless power transfer, biomedical circuit design and testing, and ultra-low-power mixed signal circuits. He has authored several journal, conference, and magazine articles with IEEE covering these topics.

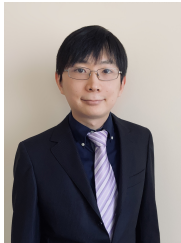


**Daniel Gulick** (Member, IEEE) received a BS in Electrical Engineering from the University of Virginia in 2008, and a Ph.D. in Biomedical Engineering from Arizona State University in 2015. He currently works at ASU as an Associate Research Scientist. His research interests include micro-sized fluid valves for hydrocephalus and glaucoma treatment, wireless power transfer to implanted devices, chipless RFID sensors, and ultrasound bioeffects on brain and nerves.



**Diogo Moniz-Garcia, M.D.** obtained his medical school training at the University of Porto, Portugal in 2019 and is currently a post-doctoral research fellow at the Mayo Clinic Florida Neurosurgery Department. His research focuses on translational efforts to maximize the clinical benefits of surgery in the operating room, including the optimization of new technologies to maximize safe resection in brain tumors, novel personalized approaches to query therapeutic vulnerability profiling of malignant neoplasms and development of novel medical

devices.



**Shiyi Liu** (Member, IEEE) was born in Beijing, China, in 1989. He received the B.Sc. and M.Sc degrees from Tianjin University, China, in 2011 and 2013 respectively. He obtained a Ph.D. in Electrical Engineering from Arizona State University in 2020, where he continued to work as a Postdoc Researcher for 2 years. His research focused on RF circuits, MEMS sensors, and microelectronic devices for biomedical applications, and particularly, wireless electronic systems for brain implants. He is currently an RF Module Design Engineer at Skyworks Solu-

tions, Inc.



**Alfredo Quinones-Hinojosa, M.D.** is the William J. and Charles H. Mayo Professor, the Monica Flynn Jacoby Endowed Chair of Neurosurgery and the James C. and Sarah K. Kennedy Dean of Research at the Mayo Clinic Florida. He leads the Brain Tumor Stem Cell Laboratory, an NIH-funded laboratory devoted to furthering our collective understanding of malignant brain tumors. Dr. Quinones has led multiple multi-institutional federal grants, clinical trials and holds multiple patents for new medical devices.

His research focuses on leveraging the operating room as his laboratory and to study brain tumors from a clinical, surgical and basic perspective aimed at translational impact to improve patient outcomes.



**Jennifer M. Blain Christen** (Senior Member, IEEE) received a Ph.D. degree in electrical and computer engineering from the Johns Hopkins University, Baltimore, MD, USA, in 2007. She completed a post-doctoral fellowship at the Johns Hopkins School of Medicine in the Department of Immunogenetics in 2008. She joined the Faculty of the School of Electrical, Computer, and Energy Engineering and Arizona State University, Tempe, AZ, USA in 2008. Her research interests include point of care diagnostics for underserved populations, wireless implantable

medical devices, and highly deployable technology for planetary and human health. She was the recipient of a 2016 NSF CAREER Award, 2020 Fulton Entrepreneurial Professorship, and 2021 Flinn Foundation Translational Bioscience awardee. She has served on the Board of Governors for the Circuits and Systems (CAS) Society and Chair of the CAS Technical Committee. She was the general co-chair of the 2023 Midwest Symposium on Circuits and Systems. She was a founding member of the Diversity and Inclusion Initiative at Arizona State University, an ADVANCE fellow, and a Fulton Schools of Engineering's Mentorship 360 Fellow. She is the co-founder of FlexBioTech, a molecular diagnostics startup, and co-founder of The Academic Life, a Faculty Development non-profit organization.